



Flow in porous media

August Geelmuyden

University of Oslo

Thanks for all the fun. I have learned a lot during these weeks!

CONTENTS

| | | |
|------------|---|-----------|
| I | Introduction | 2 |
| I.1 | The degree of wetting | 2 |
| I.2 | Drainage and imbibition | 2 |
| I.3 | The Hele-Shaw cell | 2 |
| I.4 | Dominating forces | 3 |
| I.5 | Fractal patterns | 4 |
| II | Method | 5 |
| II.1 | Fluid characteristic | 5 |
| II.2 | Circular cell | 7 |
| II.3 | Rectangular cell | 7 |
| III | Analysis | 8 |
| III.1 | Pattern extraction | 8 |
| III.2 | Box counting | 9 |
| IV | Results and discussion | 9 |
| IV.1 | Pattern formation and injection speed | 9 |
| IV.2 | Pattern change in circular cell | 10 |
| IV.3 | Gravity effects | 11 |
| IV.4 | Fractal dimensions | 15 |
| V | Conclusion | 17 |

I. INTRODUCTION

The wetting of dry materials and drainage of wet materials are omnipresent phenomena in our daily lives. When removing unwanted fluid from an object we often resort to towels, whose main purpose is to serve as objects that are wetted easily. Most people own a rain jacket, which serves as protection from fluid by its ability not to be wetted. The material *polytetrafluoroethylene*, or *teflon*, has become a standard coating of pans and other cookware due to its hydrophobic properties. Knowing that the process of wetting and drainage is ubiquitous, it is natural to wonder exactly what physical properties are relevant for the two processes. The perhaps most interesting case is where the medium subjected to wetting is porous. That is, the material contains pores which can be invaded by a fluid. Examples of such phenomena range from the watering of soil and drying of textiles, to extraction of oil from micropores and the flow of air in our lungs. In this text, the physics of these processes will be investigated. Before doing so, however, we should first extend our vocabulary.

I.1. THE DEGREE OF WETTING

A solid object is said to be wet when a fluid maintains contact with it. In that case the fluid is ascribed the property of *wetting* with respect to the material of the object. More formally, we can for a droplet of any fluid on a plane of any solid material define the *contact angle* by the angle subtended by the plane and the tangent of the fluid's surface at the point where the three phases, gas, liquid and solid meet. Conventionally, this angle is measured through the liquid as shown in figure 1.



Figure 1: The contact angle defining the wettability of a solid by a fluid.

We say that the wettability of a solid with respect to a fluid is the contact angle θ . If $\theta < 90^\circ$ the liquid is said to be wetting the solid, and if $\theta > 90^\circ$ the liquid is said to be non-wetting.

I.2. DRAINAGE AND IMBIBITION

When considering the invasion of a porous medium by a fluid, it is natural to make a distinction of two very different cases. If the porous medium is occupied by a non-wetting fluid and the invading fluid is wetting, then the process is referred to as *imbibition*. Oppositely, if a wetted porous medium is invaded by a non-wetting fluid the process is referred to as *drainage*.

I.3. THE HELE-SHAW CELL

To make the process more easy to study, we consider flow confined between two plates. If the plates can be assumed to have an infinitesimal separation and the advective intertial flow is dominated by viscous forces the flow is referred to as *Hele-Shaw flow* and the flow configuration as a *Hele-Shaw cell*. In that case, the flow can be described by Darcy's law, stating that

$$\mathbf{u} = -\frac{\kappa}{\mu} (\nabla p - \rho g) \quad (1)$$

where \mathbf{u} is the flux per unit cross sectional area, μ is the dynamic viscosity of the fluid and κ is some constant referred to as the *permeability* of the medium. As you might have guessed, ρ is the mass density of the fluid, \mathbf{g} is the acceleration due to gravity and p is the pressure.

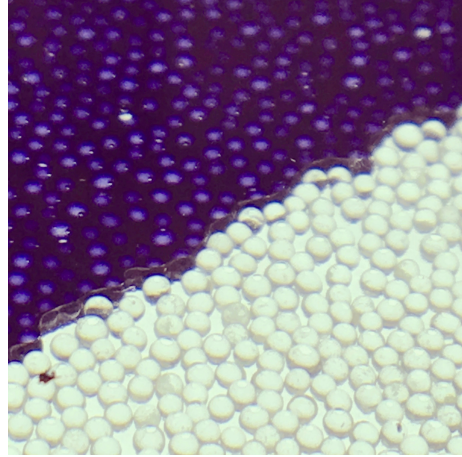


Figure 2: The invasion front of the wetting phase during imbibition of a Hele-Shaw cell filled with glass beads.

Here, it is worth noticing that if the considered fluid is incompressible, and with uniform viscosity, permeability and density, then

$$\nabla \cdot \mathbf{u} = -\frac{\kappa}{\mu} (\nabla^2 p - \rho \nabla \cdot \mathbf{g}) = -\frac{\kappa}{\mu} \nabla^2 p = 0.$$

Clearly, the approximation $\nabla \cdot \mathbf{g} = 0$ holds for any Hele-Shaw cell of reasonable size. This means that the flux per unit area of any incompressible fluid satisfying Darcy's law will satisfy Laplace's equation.

I.4. DOMINATING FORCES

Throughout our discussion so far, we have silently assumed the two fluids to be immiscible. The interface separating the two fluids is what we have denoted as the *invasion front*. If this interface attains a curvature, then surely it must be by virtue of some force that is able to balance out the force due to surface tension. This force we may represent as a pressure difference Δp across the interface. In the equilibrium situation these forces balance perfectly, meaning that

$$\Delta p = -\gamma \nabla \cdot \mathbf{n} = \gamma 2H$$

where \mathbf{n} is a unit normal vector to the interface and H is the mean curvature of the interface. We may express the mean curvature as the mean of the principal curvatures as $2H = \frac{1}{R_1} + \frac{1}{R_2}$, where R_1 and R_2 is the maximal and minimal radius of curvature of the interface. That is

$$\Delta p = \gamma \left(\frac{1}{R_1} + \frac{1}{R_2} \right), \quad (2)$$

which is referred to as the Young-Laplace equation. If we assume the invasion front to be moving due to some applied force to the system, we expect the fronts invasion of a pore to be as illustrated in figure 3.

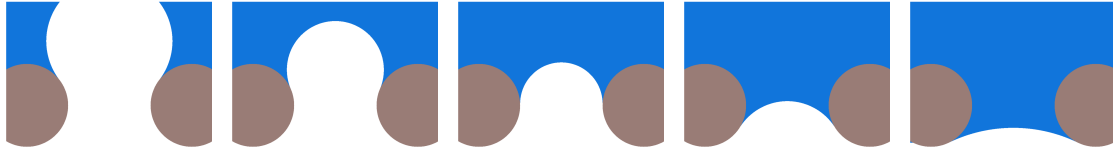


Figure 3: Sequential illustration of the evolution of the invasion front.

Now, pretending the interface has a uniform curvature given by the radius of curvature r , the Young-Laplace equation simplifies to

$$\Delta p = \frac{2\gamma}{r}.$$

By virtue of this simplification it is, by looking at figure 3, easy to convince ourselves that the maximal pressure difference is acquired when the radius of curvature equals half the poresize. Generally, if R is half the poresize, then $R = r \cos \theta$ where r is the radius of curvature and θ is the contact angle. Hence, the maximal pressure across the interface is

$$\Delta P_{thr} = \frac{2\gamma \cos \theta}{R}. \quad (3)$$

This pressure, which makes sense also when R is not minimal, is the so-called *capillary pressure*.

When a fluid creeps through the medium at high speeds, it will experience an unwillingness to move due to frictional interaction with the cell. The opposing force will become weaker for points in the fluid being further away from contact with the cell. Actually, if y is the distance from the material of the cell, we define a *Newtonian fluid* as a fluid in which the opposing force F per unit area is linearly proportional with the ratio u/y of velocity of the fluid per distance to the cell. The constant of proportionality is referred to as the *dynamic viscosity* and given the symbol μ . This means that Darcy's law (1) is an equation for the viscous forces. This can be more conveniently written

$$\nabla p = -\frac{\mu}{\kappa} u + \rho g. \quad (4)$$

A small virtual displacement δr in the direction of flow amounts to a change

$$\Delta p = \nabla p \cdot \delta r = -\frac{\mu}{\kappa} u \cdot \delta r + \rho g \cdot \delta r = -\frac{\mu}{\kappa} u \delta r + \rho g \cdot \delta r$$

in pressure, where δr is to be understood as the length of the displacement vector δr . In the absence of a gravitational field, the pressure difference over a small displacement δr due to viscous forces is

$$\Delta p = -\frac{\mu u \delta r}{\kappa}. \quad (5)$$

It is important to pay notice to the fact that the two forces described above, namely capillary forces and viscous forces appear only as opposing forces to an applied force that drives the system.

I.5. FRACTAL PATTERNS

Consider the question: "How long is the coast of Norway?". It is reasonable to assume an answer exists. One could simply choose a ruler and trace the coast piece by piece. If the ruler has length δ ,

the length of the coast would then have length $N\delta$, where N is the number of rulers needed to trace the entire coast. One might imagine the length measurement to converge towards the true length of the coastline as this process is repeated for smaller values of δ . This is, however, not the case. The ruler, being straight, cannot capture the complex contour of the coastline at any length scale. As δ approaches zero, the number N of rulers will grow faster than the decline of δ making the limit value divergent. In this sense, the coast of Norway does not possess the property length.



Figure 4: The length of the coast of Norway depends on the length of the ruler.

In a sense, the coast of Norway does not possess length as it is not a one dimensional object. If we consider the dimension d of an object to be the exponent of the length scale it scales with, we may measure the size of this object by calculating $\gamma_d N(\delta)\delta^d$, where γ_d is some possible prefactor, when δ goes to zero. Note that there can be only one value of d for which this notion of size has a finite value. That is, some object of dimension D has size M_D if

$$M_d = \lim_{\delta \rightarrow 0} \gamma(d)N(\delta)\delta^d = \begin{cases} 0 & \text{for } d > D \\ \infty & \text{for } d < D \end{cases}. \quad (6)$$

This dimension is commonly referred to as the *Hausdorff-Besicovitch* dimension. Formally, we say that a figure is a *fractal* if its Hausdorff-Besicovitch dimension exceeds its topological dimension. The topological dimension should here be qualitatively understood as the concept of dimension we are familiar with. If talking about a fractal, it is customary to label its Hausdorff-Besicovitch dimension as its *fractal dimension*.

II. METHOD

II.1. FLUID CHARACTERISTIC

The fluid used in the experiments is a 80%-20% glycerol-water solution by weight. To better visualize the flow, some water soluble nigrosin is added to color the fluid black. A weight measurement of $V = 51.004\text{cm}^3$ of the fluid yields the value 61.644g , meaning that the density of the fluid is measured to be

$$\rho = 1.209\text{g/cm}^3.$$

When measuring the viscosity with a viscometer, four values displayed in table 1 can be used together with the provided calibration constant $\kappa = 0.11127\text{mm}^2/\text{s}^2$ to find the kinematic viscosity

$$\nu = \kappa t = 36.79\text{mm}^2/\text{s} \pm 2\%.$$

Table 1: The four measured times for the fluid to travel through the viscometer.

| t[m.s] | 5.28.09 | 5.30.17 | 5.30.22 | 5.33.90 |
|--------|---------|---------|---------|---------|
| | | | | |

This makes us able to calculate the dynamic viscosity

$$\mu = 0.044 \text{ sPa} \pm 2\%.$$

The contact angle for the fluid relative to glass and air was found to be 56.6° using a goniometer as displayed in figure 5.



Figure 5: The contact angle between the 80-20 glycerol-water solution, glass and air was found to be 56.6° using a goniometer.

The surface tension of the fluid is measured both using a goniometer and by observing its capillary rise in a glass tube. In the leftmost image of figure 6, the outer diameter is estimated to be $d_o = 808 \text{ px}$ while the inner diameter is $d_i = 520 \text{ px}$. Knowing that the outer diameter of the tube is 1.65 mm we thus find the inner radius to be $R = 0.53 \text{ mm}$. By invoking equation (3) we can then estimate the surface tension by

$$\gamma = \frac{\rho ghR}{2 \cos \theta} \approx 51 \text{ mN/m}.$$

having used the same pixel-counting method for estimating $h = 9 \text{ mm}$. This does not agree well with the measured value 64.58 mN/m using the goniometer.

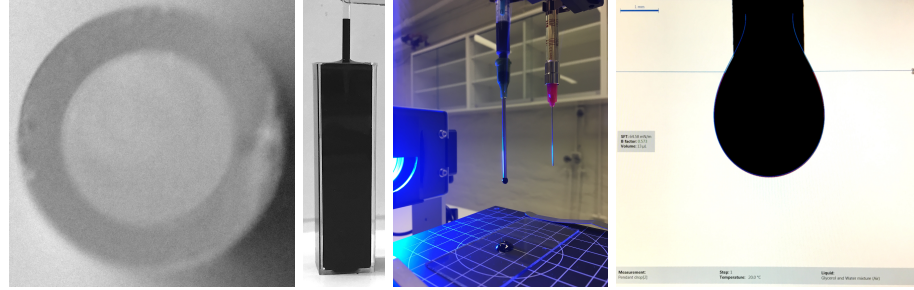


Figure 6: The surface tension was measured in two ways. The leftmost pair displays the measurement of the capillary rise, while the rightmost pair shows how the surface tension was measured using a goniometer.

II.2. CIRCULAR CELL

The setup for the experiments done with the circular Hele-Shaw cell is shown in figure 7. Here, beads with diameter 1mm were distributed randomly in monolayer between two sheets of plastic contact paper. The contact paper was glued to a circular glass disc with a central hole so that when fluid is injected into the hole, it needs to pass through the monolayer. The other side of the cell is placed on another glass plate with a plastic water repository inbetween. By manipulating the pressure in the water repository, the flow is properly confined to within the cell.

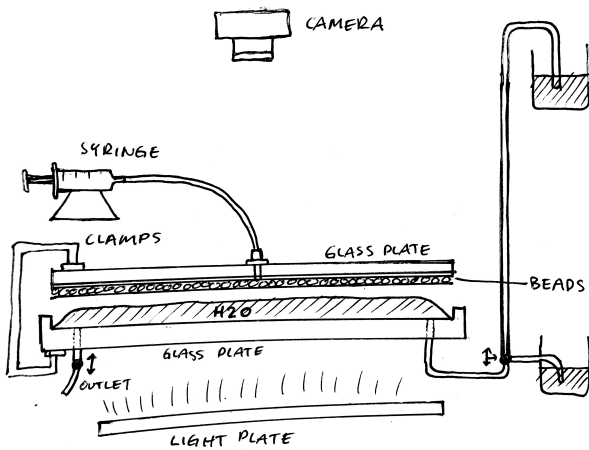


Figure 7: The experimental setup for the circular Hele-Shaw cell.

Underneath the contraption a flicker-free light plate is positioned to improve on the images taken from the camera positioned on the other side.

The experiment amounts to first filling the cell with fluid using the syringe. This imbibition process is not discussed in this text. Once the cell is reasonably full, the experiment is started by injecting air into the cell from the syringe.

II.3. RECTANGULAR CELL

The rectangular cell is, unlike the circular, not remade for each experiment. The beads in the cell is kept fixed such that in a new experiment, one need only refill the cell with fluid. Another difference is the flow direction, which is not radial, but parallel. In figure 8 one may also see that this cell has an adjustable inclination angle. This can be used to study the gravity effects on the flow.

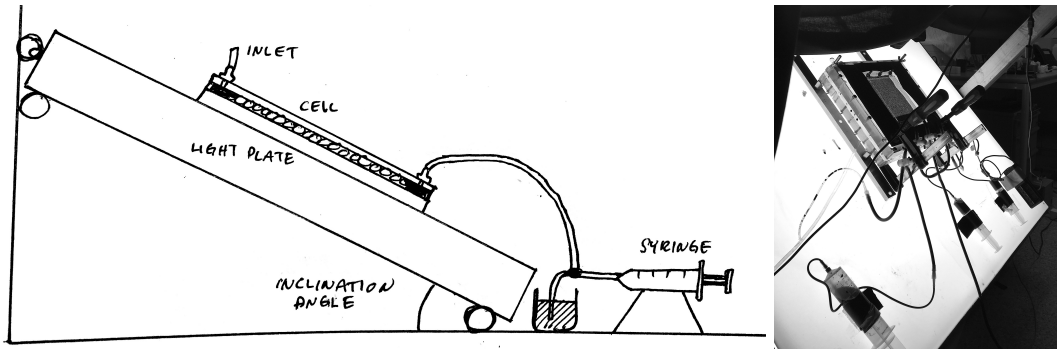


Figure 8: The experimental setup for the rectangular Hele-Shaw cell.

A rather important difference from the circular Hele-Shaw cell is the driving force. In the circular cell, air is pushed into the model using a syringe. In the rectangular model, on the other hand, the fluid is *extracted* from the cell. This reduces the effects arising from the compressibility of air.

III. ANALYSIS

III.1. PATTERN EXTRACTION

Even though the invasion pattern is clear to the eye, it is necessary to filter out everything that is not part of the pattern. This is done by choosing a reference image from the initial setup which represents the things in the image we want to remove. From any image of the experiment at a later time this initial image should then be subtracted to form a difference image. This image is then converted to a boolean image by choosing a threshold pixel value. Since the light intensity and direction may have changed during the experiment, the overall intensity and light reflection from the beads may be different in the two images. This means that we should expect to see noise in the boolean image. To get rid of this noise the method of binary erosion and dilation is used. The idea is to erode the boundary of the boolean image by some chosen radius larger than the typical noise size, but smaller than the pattern width. After having done this, the image is restored by expanding the remaining boundaries with the same radius as in the erosion. In an attempt to capture the time-evolution of the experiment, one may calculate an average of the boolean images to form a color gradient. Clearly, this works only in experiments that do not experience any snap-off, i.e. invaded pores that are reclaimed by the fluid.

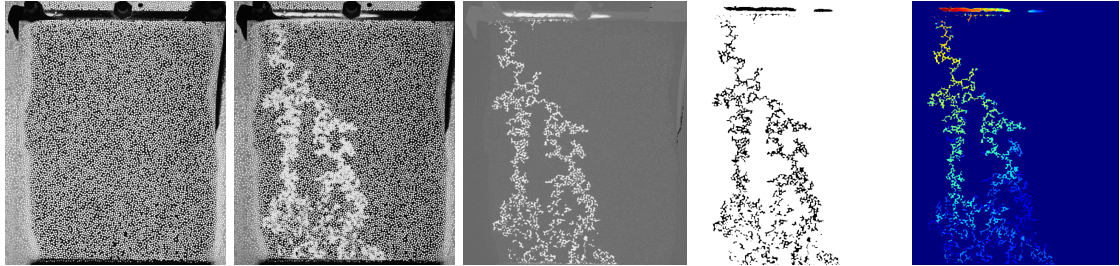


Figure 9: The different stages in the analysis of an experiment: the initial image, some image of the ongoing experiment, the difference of the images, the eroded and dilated boolean image and the invasion matrix.

III.2. BOX COUNTING

That the defining equation (6) does not proclaim the fractal dimension D to be an integer should be noted as one of the key properties of a fractal. To calculate the fractal dimension it is nice to first notice that for small values of δ ,

$$N(\delta) = A\delta^{-D} \quad (7)$$

for some constant A . Applying the logarithm to both sides of this equation yields the relation

$$\log N = -D \log \delta + \log A,$$

meaning that the fractal dimension D is found from the slope of the relation between $\log \delta$ and $\log N$ for small values of δ .

There is one problem with this approach: how do we interpret the limit $\delta \rightarrow 0$ physically? The remedy is, as usual, found from the choice of a reference scale δ^* so that δ/δ^* is unitless. Using this interpretation $\delta \rightarrow 0$ simply means that δ is to be taken much smaller as the structure as a whole, but possibly bigger than the resolution of the pattern. To calculate the fractal dimension of the Norwegian map for instance, we need only consider the map at different resolutions, and count the number of pixels containing parts of the map. The logarithm of these numbers will be linearly related, with the negative slope being the fractal dimension.

IV. RESULTS AND DISCUSSION

IV.1. PATTERN FORMATION AND INJECTION SPEED

In figure 10 the resulting pattern from two experiments with different injection speeds in the circular Hele-Shaw cell is depicted. Clearly, the slow experiment displaces much more fluid on its way out of the cell than the fast one.

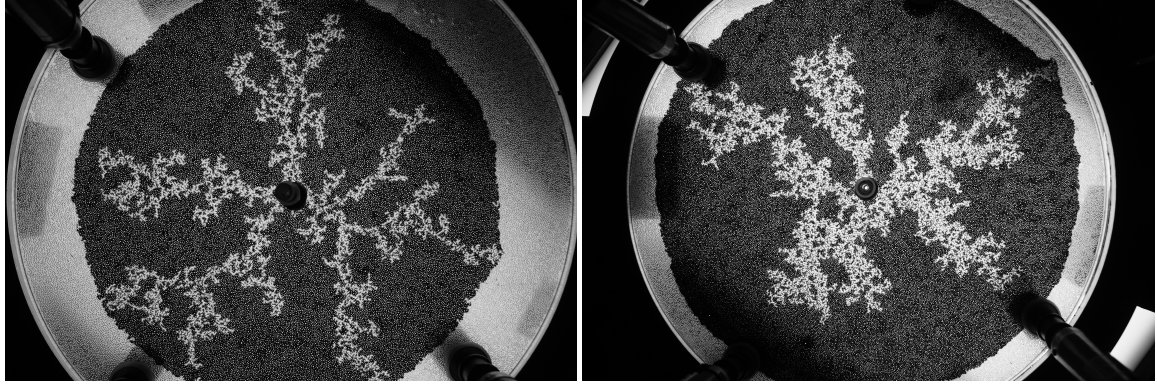


Figure 10: The experiments with different injection speeds. In the experiment depicted to the left 35 ml of air was injected per minute. To the right, the rate was decreased to 20 ml/min.

A possible explanation is seen by first recalling the discussion of the forces involved in the process. When the injection speed increases, so does the flux per unit volume (u) in the cell. Since only the viscous forces depend on velocity, we infer that in the fast experiment the viscous forces are more dominant. The key insight is found from considering the direction of the two forces. The force due to viscosity acts in the direction of movement, while the capillary force acts in any direction as long as it is across a fluid interface. Hence it is not so surprising that the width of the pattern front decreases with increasing injection speed. Often, the pattern of the displacing fluid is referred to as *fingers*. In that terminology, the fast experiments are referred to as *viscous fingering* and the slow experiments *capillary fingering*.

There is more to the story though. In the justification above, we argued that the viscous fingers appear as a consequence of the direction of the viscous force. The problem is that equation (5) does not make sense across a fluid interface. When considering the virtual displacement $\delta\mathbf{r}$ across an interface, then surely we must change the viscosity as well. Hence the equation should be restated in the form

$$\Delta p = -\frac{u\delta r}{\kappa} \Delta \mu.$$

But then Δp is positive when $\Delta \mu$ is negative, indicating that if the displaced fluid is less viscous, then the viscous forces act away from the boundary and thus preventing the creation of viscous fingers. In our case, however, the viscosity of the displaced fluid (glycerol-water) is greater than the injected fluid (air) meaning that $\Delta \mu > 0$ when considering virtual displacements outwards. Hence thinner fingers is expected for faster injection rates.

IV.2. PATTERN CHANGE IN CIRCULAR CELL

In the pattern produced by the slow experiment (20ml/min) in the circular cell one might spot a curious effect that is worth mentioning. Consider the pattern in figure 11. As the air continues to displace the fluid along its path to the periphery, the width of the front seems to narrow. Recycling the arguments performed in the previous section we are tempted to conclude that the velocity of the front increases as a function of the distance from the injection point.



Figure 11: The pattern produced by the slow experiment, 20ml/min, in the circular cell.

To understand what is going on, we should recall what drives the system. The time evolution of the system is driven by a syringe that injects air into, and thus increases the pressure in, the center of the cell. Any spontaneous movement of the liquid inside the cell must be towards a state that is closer to equalizing its surrounding pressure. When the front starts invading from the center, the distance to the boundary is large. Hence the difference in pressure across the fluid per separation distance is small. When the separation distance increases, then so must the fluid's willingness to engage in spontaneous movement towards the rim of the cell. This effect is neatly woven into Darcy's law where the flux per unit cross sectional area \mathbf{u} is proportional with the pressure gradient in the absence of a gravitational field. Assuming the system to be reasonably close to equilibrium, the pressure gradient should distribute linearly over the fluid and thus be proportional to the reciprocal of the distance of separation.

Curiously, this implies that the outer boundary of the displaced fluid will evolve towards a shape that is not circular. When the invading air is close to the rim, its velocity increases rapidly. Being incompressible, the fluid has to go somewhere, and at some point it does not have time to align to form a perfect circle. The exact physics of the deformation of the circle would perhaps be an interesting study of the interplay of drainage and imbibition.

It should here be noted that the effects discussed above only concern the circular cell.

IV.3. GRAVITY EFFECTS

When tilting the model, the contribution from gravity in Darcy's law is no longer negligible. The pressure drop along a virtual displacement $\delta\mathbf{r}$ is thus dependent on its overlap with the direction

of acceleration due to gravity. Since the invasion happens downwards, as illustrated in figure 8, the contribution from the term $\rho g \cdot \delta r$ is positive. Hence the effect of gravity is counter to that of viscous fingering.

When the fluid withdrawal is fast, however, the viscous forces should dominate the pattern formation. That is, when $\frac{\Delta\mu}{\kappa} \nabla p$ is big, then $\rho g \cdot \delta r$ will be negligible. This can be seen from figure 12, where two equally fast experiments were done without inclination and with 45° inclination. Which of the resulting patterns happens to be the one with gravity effects is difficult to tell. One has to look closely to realize that the fingers in the rightmost pattern is slightly larger than those of the one to the left.

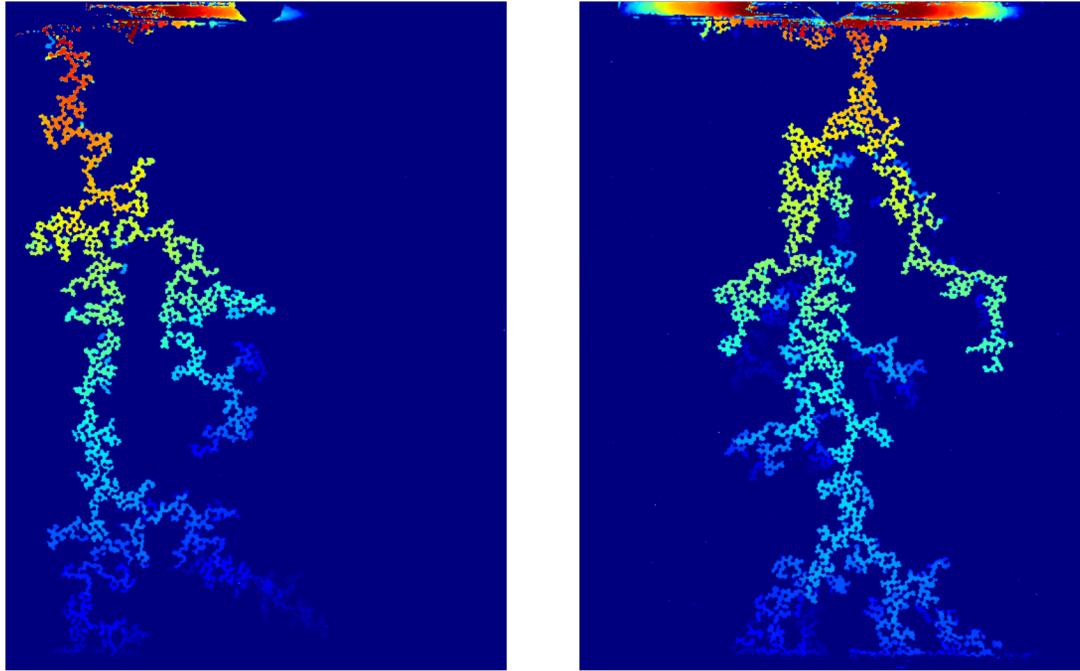


Figure 12: The time evolution of the pattern formation in the rectangular model for two fast experiments (10ml/min) at different inclinations. The leftmost has an inclination angle of 0.7° , and the other has 45.2° .

When the experiment is redone for an ultraslow experiment where only 0.06ml fluid is withdrawn from the cell per hour, the gravity contribution becomes evident. This is shown in figure 13. The pattern formation in the rightmost image seems to have evolved almost as a straight front perpendicular to the direction of propagation. This is by no means surprising. If the front has width b , then the pressure difference between the upper and the lower part of the front is given by

$$\Delta p = \rho g b \cos \theta_{inc}$$

where θ_{inc} is the inclination angle. This means that there will be some maximal number of b in which Δp starts getting positive. This should happen when the pressure difference due to gravity exceeds the capillary pressure of the pore size. That is if the upper pore has poresize R_1 and the

lower has R_2 and their height differ with h , then

$$2\gamma \cos \theta \left(\frac{1}{R_2} - \frac{1}{R_1} \right) = \rho g h.$$

One could here invoke the statistical machinery to express the expected difference $\frac{1}{R_2} - \frac{1}{R_1}$ in terms of the width of the distribution of pore sizes in the cell. Such a detailed analysis is omitted from this text, the main reason being the lack of data to test the eventual relation.

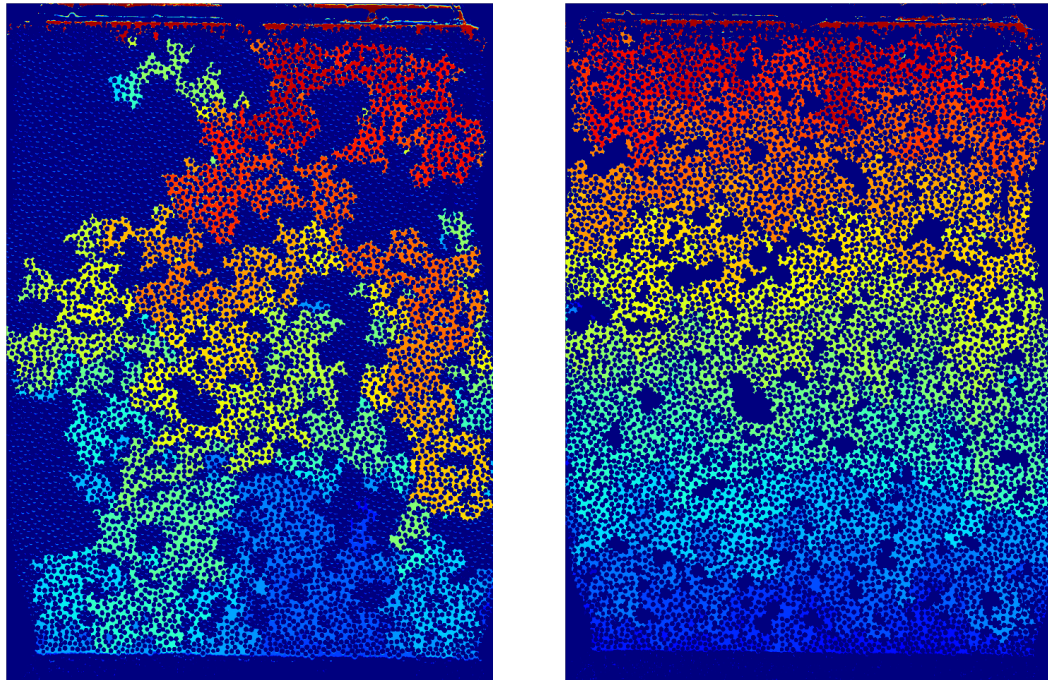


Figure 13: The time evolution of the pattern formation in the rectangular model for two slow experiments ($0.06\text{ml}/\text{h}$) at different inclinations. The leftmost has an inclination angle of 0.2° , and the other has 45.1° .

Now consider the image to the left in figure 13. Notice how the pattern seems to invade the porous medium in large chunks. This is also anticipated as the system eventually will have to confront an area where all the pores are especially small. In that case, the evolution of the front will halt until the pressure builds up to exceed the capillary pressure threshold. Having been supplied with this large "amount" of pressure, the front can now invade all of the pores in the neighbouring area.

In the lower right corner of the rectangular cell, a pressure sensor was placed to record the experiment. Even though time shortage has made it difficult to properly implement this data in the analysis, it serves to tell the story of the pattern formation from a different perspective. The pressure readings from the inclined experiment is shown in figure 14.

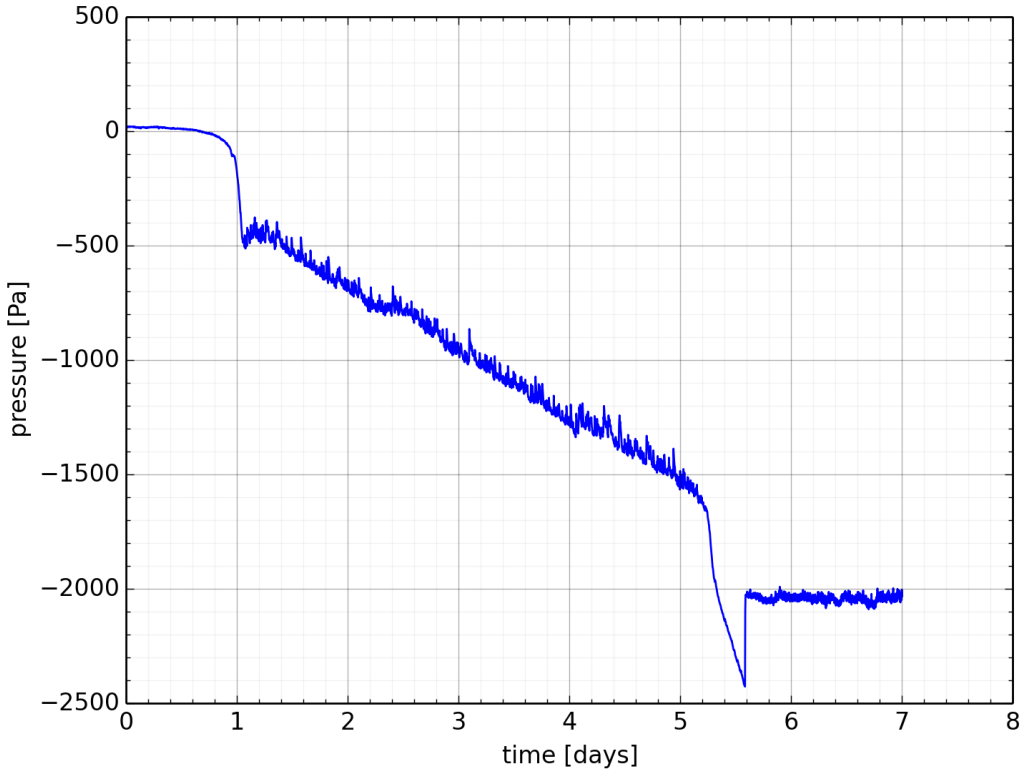


Figure 14: The pressure in the lower right corner of the cell as a function of time in the experiment to the right in figure 13. The pressure is provided in pascal and is measured relative to the pressure when the experiment started.

After having initiated the experiment, it takes one day for the system to build up a pressure that is large enough (about 500Pa) to start invading the porous medium. The invasion of the medium progresses as a sequence of bursts, as is manifest from the spiky noise in the pressure. As the front keeps on invading downwards, the pressure in the fluid due to gravity decreases. After about five days the front has passed through the medium and is blocked from further invasion by the sponge separating the outlet from the bottom of the model. Due to the much smaller pores in the sponge, the system need yet another build-up of pressure before being able to invade further downwards through the sponge. The removal of fluid from the sponge does, however, not concern the pressure due to gravity in the pressure sensor more than some noise indicating the new invasion of a pore in the sponge.

When considering the pressure readings from the experiment without gravity effects, the story is very similar. The main difference is the fact that the pressure does not drop as the porous medium is invaded. The beginning of the pressure curve is probably due to some excess fluid left in the inlet. The removal of this fluid will be seen by the pressure sensor as a gradual drop due to gravity effects. Having observed this, the pressure readings is shifted so that the pressure is zero when the excess fluid is gone.

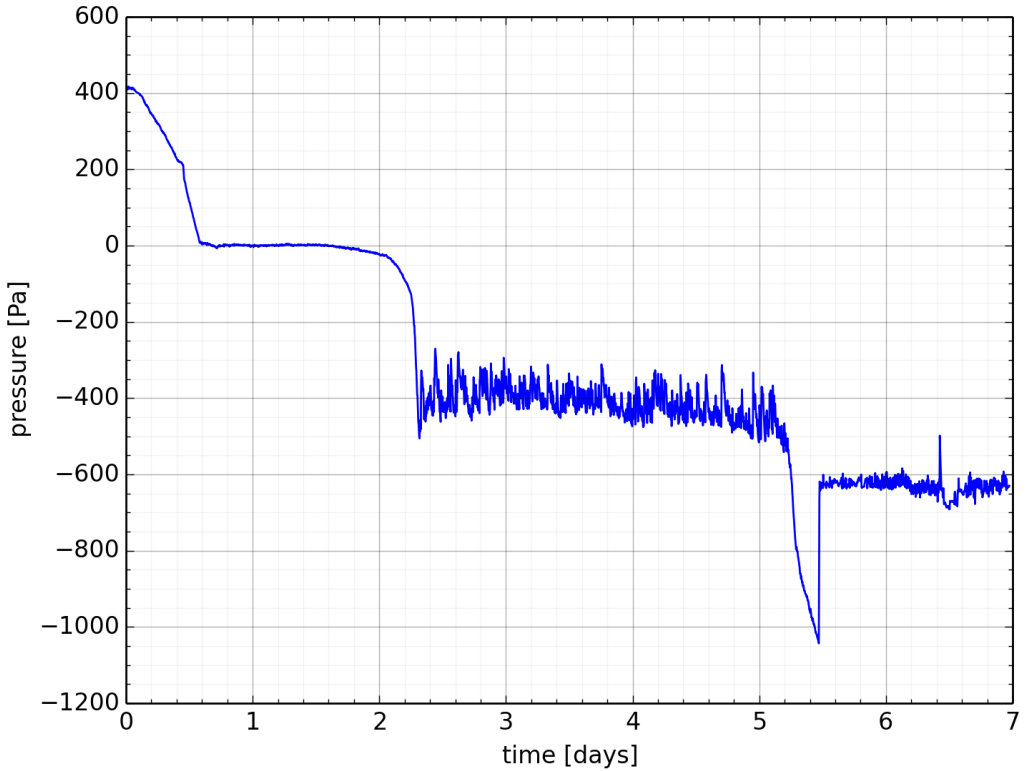


Figure 15: The pressure in the lower right corner of the cell as a function of time in the experiment to the left in figure 13. The pressure is provided in pascal and is measured relative to the pressure when the experiment started.

IV.4. FRACTAL DIMENSIONS

Lastly, we take a brief look on the fractal dimension of the various generated patterns. In figure 17 we see the result of the Box-counting method for the various experiments discussed in this text. Two additional graphs are added, namely DLA 500x500 and DLA 300x300. These refer to the patterns produced by implementing the *diffusion limited aggregation* algorithm to simulate viscous fingering. Although the justification and construction of the algorithm is omitted here, the resulting patterns are shown in figure 16.

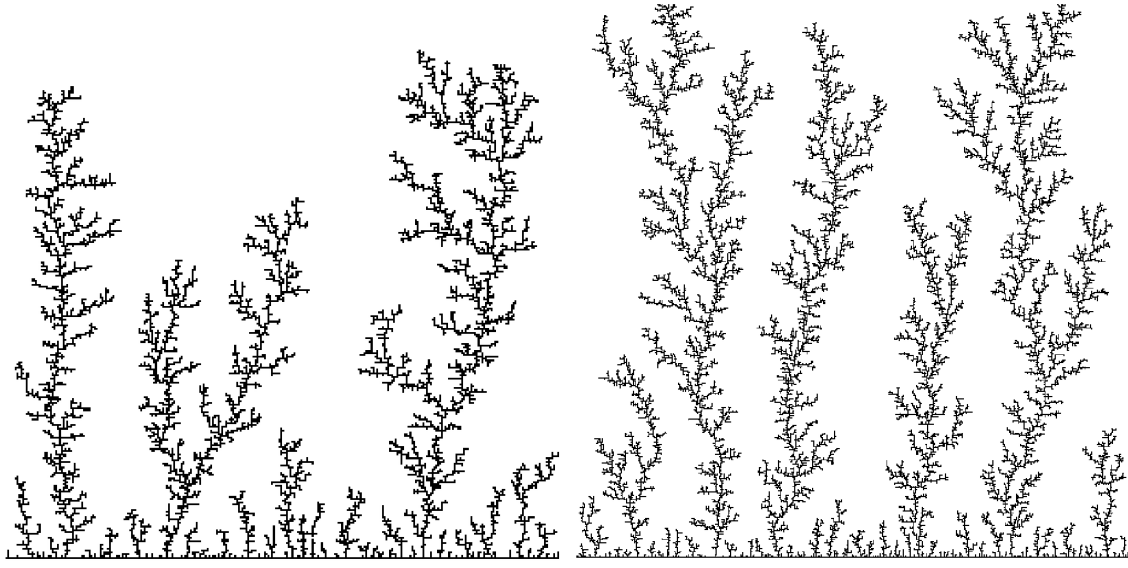


Figure 16: The patterns produced by the DLA (diffusion limited aggregation) algorithm for the resolutions 300x300 and 500x500 respectively.

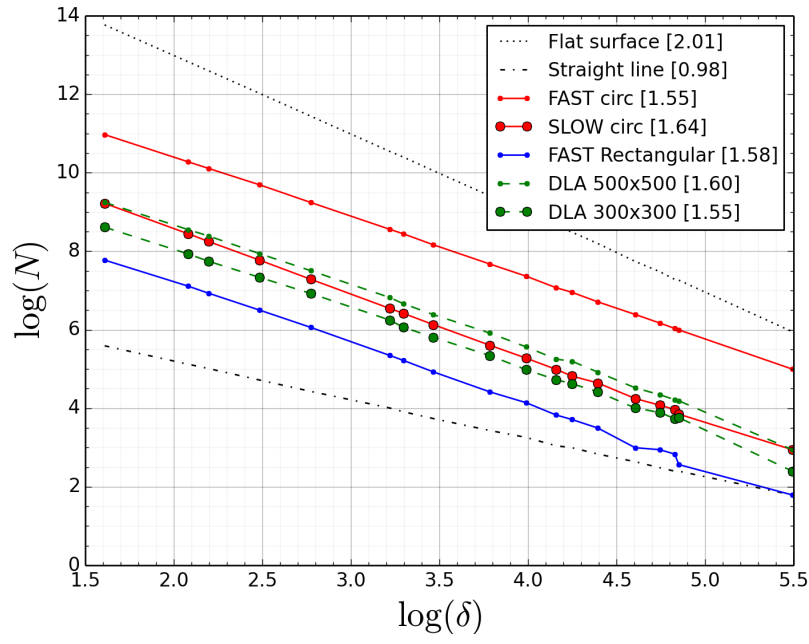


Figure 17: The scaling properties of the various patterns described in this text. For comparison, similar lines for a flat surface and a straight line is included.

As seen from figure 17, all fingering patterns seem to have approximately the same fractal dimension.

This is as expected, although the variations in injection speed should alter the fractal dimensions slightly. We have seen that as the injection speed increases, then the width of the fingers decrease. Hence the resulting pattern becomes closer to a one-dimensional object as injection speed is increased. This means that the fastest experiment, namely the 35ml/min in the circular cell, is expected to have the lowest fractal dimension. In figure 17 we can see that this is indeed the case. The different slopes is perhaps more clear when they are forced to intersect at the same point. The resulting plot is shown in figure 18.

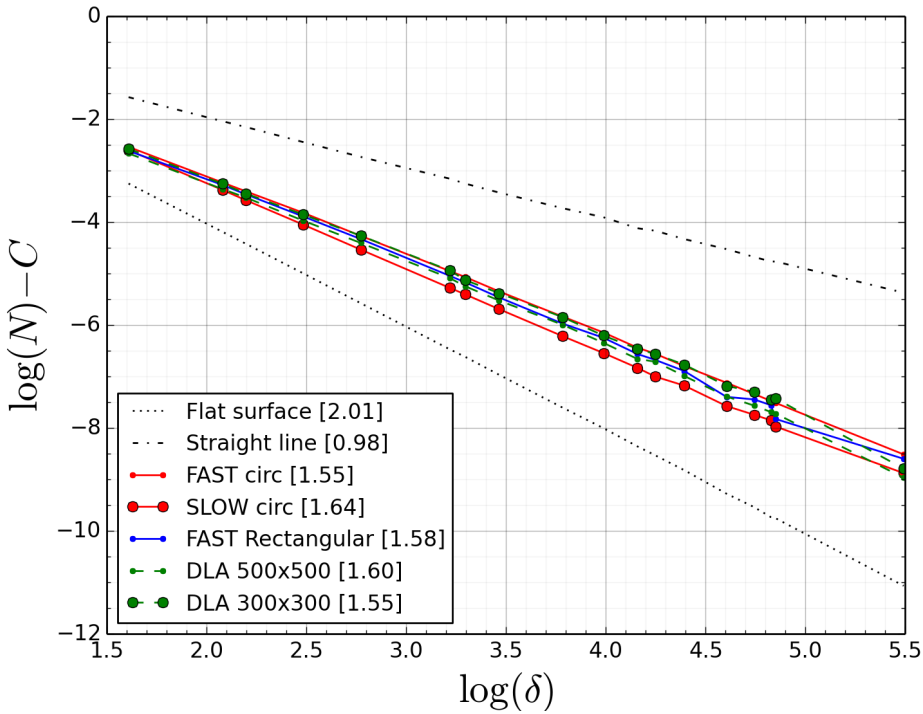


Figure 18: The scaling properties of the various patterns described in this text shifted in order to be zero at the origin.

It is reasonable to expect the fractal dimension to depend on the relative sizes of the capillary and viscous forces only. We would expect the fractal dimension to be a decreasing function of the ratio of viscous to capillary forces. To test whether this actually is the case, and if so, what the exact form of dependency is, could have been an interesting study in the presence of more data.

V. CONCLUSION

When considering drainage of porous media, the pattern formation is governed by two forces: viscous and capillary. If the displaced fluid has the largest dynamic viscosity, then the invasion front is unstable in processes dominated by the viscous forces. The relative strength of the viscous and capillary forces can be modified by changing the speed of the fluid displacement. By increasing the injection (or withdrawal) speed the viscous forces becomes more dominant leading to fractal

displacement patterns. The fractal dimension of these patterns seems to increase from 1.5 and upwards as the ratio of viscosity to capillary pressure rises.

When studying capillary fingering, the fluid displacement seems to happen by spontaneous invasions of large chunks of the medium. This is anticipated and expected to be predictable from the distribution of pore size.

As anticipated, the introduction of gravitational forces in the direction of flow has little effect on the pattern formation in the fast experiments. As the capillary forces become more important, the presence of gravitational forces has the effect of stabilizing the front of the capillary fingering. The width of the front is expected to be calculable from the distribution of pore size.

REFERENCES

- [1] Feder, Jens. *Fractals*. Springer Science & Business Media, 2013.
- [2] Moura, Marcel N. *Burst dynamics in quasi-2D disordered systems: experiments on porous media two-phase flows*. Reprocentralen, University of Oslo
- [3] Birovljev, A., et al. *Gravity invasion percolation in two dimensions: Experiment and simulation*. Physical Review Letters 67.5 (1991): 584.
- [4] Homsy, George M. *Viscous fingering in porous media*. Annual review of fluid mechanics 19.1 (1987): 271-311.